

# Persistent Homology via Ellipsoids

Sara Kališnik\*, and Bastian Rieck†, and Ana Žegarac‡

## Abstract

Persistent homology is one of the most popular methods in Topological Data Analysis. An initial step in any analysis with persistent homology involves constructing a nested sequence of simplicial complexes, called a filtration, from a point cloud. There is an abundance of different complexes to choose from, with Rips, Alpha, and witness complexes being popular choices. In this manuscript, we build a different type of a geometrically-informed simplicial complex, called an *ellipsoid complex*. This complex is based on the idea that ellipsoids aligned with tangent directions better approximate the data compared to conventional (Euclidean) balls centered at sample points that are used in the construction of Rips and Alpha complexes, for instance. We use Principal Component Analysis to estimate tangent spaces directly from samples and present algorithms as well as an implementation for computing *ellipsoid barcodes*, i.e., topological descriptors based on ellipsoid complexes. Furthermore, we conduct extensive experiments and compare ellipsoid barcodes with standard Rips barcodes. Our findings indicate that ellipsoid complexes are particularly effective for estimating homology of manifolds and spaces with bottlenecks from samples. In particular, the persistence intervals corresponding to a ground-truth topological feature are longer compared to the intervals obtained when using the Rips complex of the data. Furthermore, ellipsoid barcodes lead to better classification results in sparsely-sampled point clouds. Finally, we demonstrate that ellipsoid barcodes outperform Rips barcodes in classification tasks.

## Contents

<b>1</b>	<b>Preliminaries</b>	<b>2</b>
1.1	Filtrations and Persistent Homology . . . . .	2
<b>2</b>	<b>Ellipsoid Complexes and their Properties</b>	<b>4</b>
2.1	Ellipsoid Complexes . . . . .	4
2.2	Relation between Ellipsoid and Rips complexes . . . . .	6
<b>3</b>	<b>Persistent Homology via Ellipsoids: the Algorithm</b>	<b>6</b>
3.1	Intersection of Ellipsoids . . . . .	7
<b>4</b>	<b>Experiments</b>	<b>8</b>
4.1	Dog Bone Example . . . . .	8
4.2	Point Cloud Classification . . . . .	8
4.3	Pentagons . . . . .	11
4.4	Cyclo-octane . . . . .	12
<b>5</b>	<b>Conclusion and Future Directions</b>	<b>13</b>
<b>6</b>	<b>Acknowledgements</b>	<b>13</b>

---

\*ETH Zurich, sara.kalisnik@math.ethz.ch

†University of Fribourg, bastian.grossenbacher@unifr.ch

‡ETH Zurich, ana.zegarac@math.ethz.ch

# Introduction

Methods from computational topology have received increased attention due to their ability to capture characteristic properties of data at multiple scales, while being less reliant on the underlying metric or coordinates [Car09]. Of these, persistent homology is the most prominent [CSO14; Cha+16]. Given an unstructured dataset in the form of a point cloud, the first step of any analysis based on persistent homology involves building a *simplicial complex* on the data. To approximate the underlying shape of the dataset, a common strategy is to calculate the Čech, Rips, Alpha or witness complex on the dataset [DI12; Zom10].

While this is a good strategy in general, in practice, many real-world high-dimensional data sets that occur in actually cluster along low-dimensional manifolds. This statement is known as the manifold hypothesis and it forms a cornerstone of modern data science [FH16]. With this in mind, we build a different type of geometrically-informed simplicial complex that is tailored to samples from manifolds. In particular, we rely on the insight that *ellipsoids* elongated in tangent directions better approximate the data set than balls centered at sample points. This statement is also supported by previous work. For instance, experiments carried out in [Bre+18] demonstrate that given a sample from a variety, complexes distorted in tangent directions combined with persistent homology result in a stronger ‘topological signal’. The drawback of [Bre+18] is that the polynomials that determine the variety are needed to approximate the tangent space.

**Our contributions.** In this manuscript we do away with this restriction and define ellipsoid complexes for a general point cloud. Tangent spaces are estimated with the help of PCA directly from the sample [JC16]. We also provide algorithms and code to compute ellipsoid barcodes and carry out extensive experiments comparing them to Rips complexes. We demonstrate that:

- Working with ellipsoids is particularly suitable when the underlying space is a manifold or has bottlenecks (see Subsection 4.1). *Persistence barcodes* arising from ellipsoid complexes exhibit a larger signal-to-noise ratio; more specifically, the persistence intervals corresponding to a ground-truth topological feature are longer (as compared to the intervals obtained when using the Rips complex of the data).
- Ellipsoid barcodes lead to better classification results in sparsely sampled point clouds and, in general, allow the user to work with smaller samples confirming the theoretical results from [KL24].
- Using datasets introduced in [TMO22] we show that ellipsoid barcodes significantly outperform Rips complexes and also outperform alpha complexes generated using Distance-to-Measure as the filtration function (see Subsection 4.2) in classification tasks in all categories except one.

## 1 Preliminaries

In this section we review the definitions of simplicial complexes and filtrations of point clouds, explain how one constructs persistence modules based on point clouds and briefly explain how persistent homology works and what information about the underlying point cloud it provides.

### 1.1 Filtrations and Persistent Homology

Persistent homology is an adaptation of homology [Hat02] to the setting of point clouds, i.e., finite metric spaces that arise from applications. The concept appeared independently in the works of Frosini and Ferri [FS10], Robins [Rob00], and Edelsbrunner, Letscher and Zomorodian [ELZ02]. For an in-depth introduction to persistent homology, see [Car09; Car13]. The goal of persistent homology is to provide a bridge between discrete and non-discrete topological spaces: point clouds, being discrete topological spaces, have no non-trivial topological features. To obtain topological features, one needs to turn the point cloud into a topological space. One way to accomplish this is to assign for every parameter  $\varepsilon > 0$  a topological space, more specifically, a simplicial complex, to the point cloud and then track the *evolution* of the topological features as the parameter  $\varepsilon$  varies.

**Definition 1.1.** An **abstract simplicial complex**  $(\Sigma, V)$  is given by a set  $V$  whose elements we call **vertices** and a set  $\Sigma$  of non-empty finite subsets of  $V$ . This data satisfies the following properties: we have that (1)  $\{v\} \in \Sigma$  for all  $v \in V$ , and (2) if  $\sigma \in \Sigma$  and  $\tau \subset \sigma$ , then  $\tau \in \Sigma$ . If  $\sigma \in \Sigma$  has cardinality  $p + 1$ , we say that  $\sigma$  is a  **$p$ -simplex**, or a **simplex of dimension  $p$** . A **simplex** is a  $p$ -simplex for some  $p \in \mathbb{N}$ .

One common way of assigning a simplicial complex to a point cloud is to take the Čech complex:

**Definition 1.2.** The **Čech complex** of  $(X, d)$ ,  $\check{C}_\varepsilon(X)$  at scale  $\varepsilon$  is the abstract simplicial complex with the vertex set  $X$ , where  $\sigma = [v_0, v_1, \dots, v_n]$  is an  $n$ -simplex in  $\check{C}_\varepsilon(X)$  if and only if  $B_\varepsilon(v_0) \cap \dots \cap B_\varepsilon(v_n) \neq \emptyset$ . In other words,  $\check{C}_\varepsilon(X)$  is an abstract simplicial complex with the vertex set  $X$ , where  $v_0, v_1, \dots, v_n$  form an  $n$ -simplex precisely when the balls of radius  $\varepsilon$  centered at these points have a non-empty intersection.

The Čech complex  $\check{C}_\varepsilon(X)$  at scale  $\varepsilon$  has the same homotopy type as the union of balls grown around the data points with radius  $r$ . This follows directly from a result referred to as Nerve Theorem [Bau+22].

In applications the so-called Vietoris-Rips (or just Rips) complex is more popular because it is easier to store.

**Definition 1.3.** Given a point cloud  $X$  and a real number  $\varepsilon \geq 0$ , we define the **Rips complex of  $X$  at scale  $\varepsilon$**  to be:

$$R_\varepsilon(X) = \{\sigma \subseteq X \mid d(x, y) \leq 2\varepsilon, \forall x, y \in \sigma\}.$$

When  $X$  is clear from the context, we write just  $R_\varepsilon$  instead of  $R_\varepsilon(X)$ .

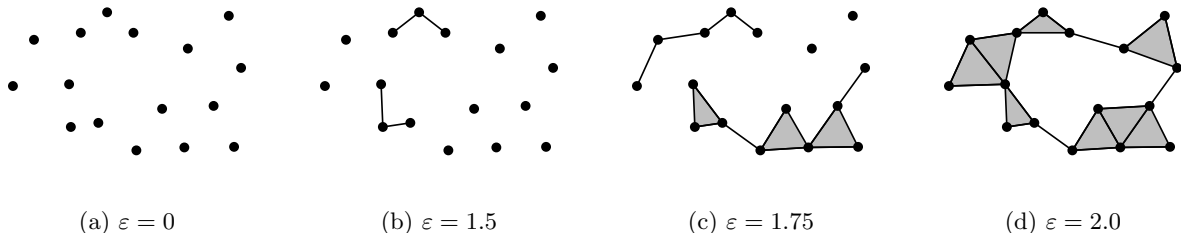


Figure 1: Four stages of a Rips complex construction for a point cloud, showing simplices up to dimension 2.

For each  $\varepsilon \leq \varepsilon'$  we have an inclusion  $\check{C}_\varepsilon(X) \hookrightarrow \check{C}_{\varepsilon'}(X)$  as well as an inclusion  $R_\varepsilon(X) \hookrightarrow R_{\varepsilon'}(X)$ . Figure 1 illustrates the Rips complex construction for the point cloud depicted in Figure 1(a). Taking a family of Rips or Čech complexes indexed over real  $\varepsilon \geq 0$  yields a filtered simplicial complex.

**Definition 1.4.** A **filtered simplicial complex** is a collection  $K = \{K_\varepsilon\}_{\varepsilon \in \mathbb{R}_{\geq 0}}$  of simplicial complexes indexed by non-negative real numbers with the property that  $K_\varepsilon \subset K_{\varepsilon'}$  whenever  $\varepsilon \leq \varepsilon'$ .

Applying the homology functor  $H_k$  in degree  $k$  to a filtered simplicial complex, we obtain what is called a ‘persistence module’ [Car13].

**Definition 1.5.** A **persistence module  $\mathbf{V}$**  is a collection of indexed vector spaces  $\{V_t \mid t \in \mathbb{R}\}$  and linear maps  $\{v_a^b \mid v_a^b: V_a \rightarrow V_b, a \leq b\}$  such that the composition has the properties  $v_b^c \circ v_a^b = v_a^c$  whenever  $a \leq b \leq c$  and  $v_b^a$  is the identity map whenever  $a = b$ .

The basic building blocks in the theory of persistence modules are interval modules.

**Definition 1.6.** For an interval  $[b, d)$  we denote by  $\mathbb{I}_{[b, d)}$  the persistence module

$$(\mathbb{I}_{[b, d)})_t = \begin{cases} \mathbf{k} & \text{for } t \in [b, d) \\ 0 & \text{otherwise} \end{cases} \quad \text{and} \quad i_t^s = \begin{cases} \text{id}_{\mathbf{k}} & \text{for } s \leq t, \text{ and } s, t \in [b, d) \\ 0 & \text{otherwise} \end{cases}.$$

The lifespan of  $\mathbb{I}_{[b, d)}$  is  $d - b$ .

The celebrated **decomposition theorem** guarantees that persistence vector modules that arise from Rips and Čech complexes and similar filtrations built on point clouds can be expressed as direct sums of ‘interval modules’.

**Theorem 1.7.** *Let  $X$  be a finite metric space and  $\{R_\varepsilon\}_{\varepsilon \in \mathbb{R}_{\geq 0}}$  the Rips filtration associated to  $X$ . Then the persistence module  $\{H_k(R_\varepsilon)\}_{\varepsilon \in \mathbb{R}_{\geq 0}}$  over  $\mathbf{k}$  can be decomposed as*

$$V \cong \bigoplus_{l \in L} \mathbb{I}_{(b_l, d_l]}.$$

The  $k$ -dimensional **barcode** associated to  $X$  is

$$\{(b_1, d_1), (b_2, d_2), \dots, (b_l, d_l)\}.$$

**Remark 1.8.** *Instead of Rips complexes we can also use filtrations arising from Čech complexes, ellipsoid complexes (which we define in Section 2.1, etc).*

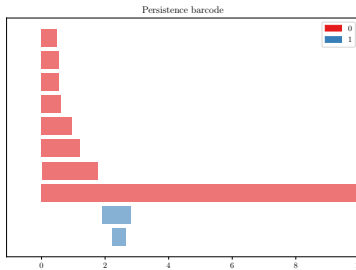


Figure 2: The Rips barcode for the point cloud depicted in Figure 1(a).

Hence the output of persistent homology on a point cloud  $X$  is a *barcode*, i.e., a collection of intervals. Each interval in the barcode corresponds to a topological feature in the filtration which appears at the value of a parameter given by the left hand endpoint of the interval and disappears at the value given by the right hand endpoint. See Figure 2 for an illustration.

## 2 Ellipsoid Complexes and their Properties

Previous experiments [Bre+18] with ellipsoid-driven complexes in combination with persistent homology suggest that in case we have a sample from a variety and if we have access to its tangent space, elongating balls in the definition of the Čech complex in the tangent direction ‘strengthens’ the topological signal. Informally speaking, using ellipsoids instead of balls makes the intervals that correspond to topological features of the point cloud longer. These complexes, however, use polynomials to access the tangent space. Furthermore, the results of [KL24] imply that by using elongated shapes one can reduce the size of the sample from the manifold while still keeping the theoretical guarantees about the shape of the underlying space (in the case of closed smooth manifolds, at least).

In this section we define ellipsoid complexes for finite subsets of Euclidean space (thus generalizing the definitions from [Bre+18]) and explore their properties.

### 2.1 Ellipsoid Complexes

**The Topological Setting.** Inspired by [KL24] we first provide definitions for ellipsoid complexes for the ideal setting, where we have a finite sample  $X$  from a known  $\mathcal{C}^1$ -submanifold  $\mathcal{M}$  of  $\mathbb{R}^n$ . A **tangent-normal coordinate system** at  $x \in \mathcal{M}$  is an  $n$ -dimensional orthonormal coordinate system with the origin in  $x$ , the first  $m$  coordinate axes tangent to  $\mathcal{M}$  at  $x$  and the last  $n - m$  axes normal to  $\mathcal{M}$  at  $x$ .

**Definition 2.1.** Let  $\mathcal{M}$  be a  $C^1$ -submanifold of  $\mathbb{R}^n$  and  $\varepsilon \in \mathbb{R}_{>0}$ . The **tangent-normal  $q$ -ellipsoid at scale  $\varepsilon$  at point  $x \in \mathcal{M}$**  is the closed ellipsoid in  $\mathbb{R}^n$  with the center in  $x$ , the tangent semi-axes of length  $\varepsilon$  and the normal semi-axes of length  $b := \varepsilon/q$ . Explicitly, in a tangent-normal coordinate system at  $x$  the tangent-normal closed ellipsoids are given by

$$E_\varepsilon^q(x) := \left\{ (x_1, \dots, x_n) \in \mathbb{R}^n \mid \frac{x_1^2 + \dots + x_m^2}{\varepsilon^2} + \frac{x_{m+1}^2 + \dots + x_n^2}{b^2} \leq 1 \right\}, \quad (1)$$

where  $m$  denotes the dimension of  $\mathcal{M}$  at  $x$ . Observe that the definitions of ellipsoids depend only on the submanifold itself.

If we know  $\mathcal{M}$  and have access to its tangent space, then for each point  $x$  from the sample  $X$  and  $\varepsilon > 0$  we have an ellipsoid. One way to produce a simplicial complex is to construct a Rips-like complex, in which edges are determined by intersections of ellipsoids. One could also use a Čech like construction with including a simplex precisely when the corresponding ellipsoids intersect (like is done in [KL24]) to keep the theoretical guarantees from the nerve lemma [Bau+22], however, for computational purposes doing that is too expensive.

**Definition 2.2. (Ellipsoid Complex)** Let  $\mathcal{M}$  be a  $C^1$ -submanifold of  $\mathbb{R}^n$  and let  $(X, d)$  be a finite metric subspace of Euclidean space  $\mathbb{R}^d$ , where  $X \subset \mathcal{M}$ . For  $x \in X$  let  $E_\varepsilon^q(x)$  be the ellipsoid from Definition 2.1. The  **$q$ -ellipsoid complex of  $X$  at scale  $\varepsilon$**  is

$$E_\varepsilon^q(X) = \{ \sigma \subseteq X \mid E_\varepsilon^q(x) \cap E_\varepsilon^q(y) \neq \emptyset, \forall x, y \in \sigma \}.$$

With other words,  $E_\varepsilon^q(X)$  is an abstract simplicial complex with the vertex set  $X$ , where  $x$  and  $y$  are connected by an edge precisely when  $E_\varepsilon^q(x) \cap E_\varepsilon^q(y) \neq \emptyset$ . A higher-dimensional simplex is included if and only if all of its edges are in  $E_\varepsilon^q(X)$ . Thus, the ellipsoid complex is a flag complex, i.e., it is fully determined by its edges.

**Example 2.3.** Consider a sample  $X$  from a circle depicted in the leftmost image in Figure 2. The remaining images show the 2-ellipsoids as well as the 2-ellipsoid complexes built on  $X$  at various scales.

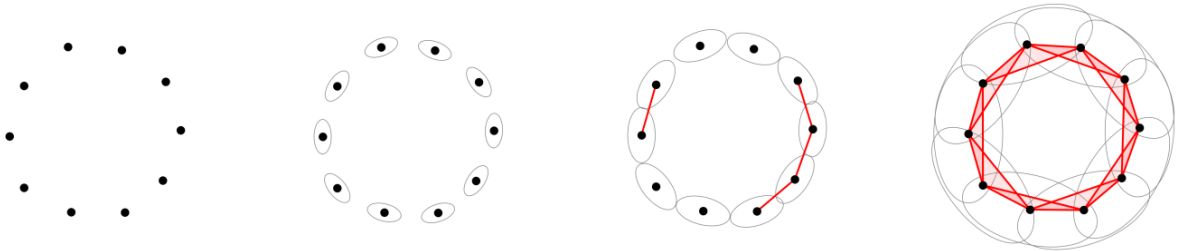


Figure 3: Four stages of an ellipsoids complex construction for a point cloud, showing simplices up to dimension 2.

**The Discrete Setting.** The main idea in passing from the topological setting to the discrete setting is that we no longer have access to the underlying manifold and its tangent spaces, but that we have to estimate them directly from the sample. To choose the orientation of each of the ellipsoids, Algorithm 1 is used.

This algorithm can be implemented efficiently using spatial data structures such as  $k$ - $d$  trees. Building such a data structure for  $n$  points in  $d$  dimensions has a worst-case complexity of  $\mathcal{O}(n \log^2 n)$ . Calculating a proper ellipsoid for each point then incurs a cost of  $\mathcal{O}(k \log n)$  for finding the  $k$  nearest neighbours, followed by  $\mathcal{O}(\min(d^3, k^3))$  for calculating principal components [JL09], with the final alignment step taking constant time. The total runtime of this algorithm is thus  $\mathcal{O}(nk \log n + n \min(d^3, k^3))$ . In lower dimensions and for sufficiently small values of  $k$ , this runtime is dominated by finding the  $k$  nearest neighbours, and we may assume that the local PCA calculations effectively run in constant time.

Given  $X$ , a finite metric subspace of  $\mathbb{R}^n$ , we denote the ellipsoid complex at scale  $\varepsilon$  with the ratio  $q$  by  $E_\varepsilon^q(X)$  and the filtration by  $E^q(X)$ . According to Theorem 1.7  $H_k(E^q(X))$  is decomposable. Unless otherwise specified we always work with ellipsoid complexes as described in the discrete setting subsection.

---

**Algorithm 1** Ellipsoid construction algorithm

---

- 1: **for each** point  $p$  in the point cloud **do**
  - 2:     Fix user-selected number  $k$  of neighbours
  - 3:     Run principal component analysis on the  $k$ -nearest neighbours of  $p$ .
  - 4:     Align the ellipsoid axes to the eigenvectors obtained from principal component analysis.
  - 5: **end for**
- 

## 2.2 Relation between Ellipsoid and Rips complexes

In this subsection we show that ellipsoid complexes can be ‘interleaved’ between Rips complexes.

**Proposition 2.4.** *Let  $X$  be a finite metric subspace of  $\mathbb{R}^n$  (with the metric inherited from  $\mathbb{R}^n$ ). Using Algorithm 1 we construct the ellipsoid complex  $E_\varepsilon^q(X)$  whose tangent semi-axes have length  $\varepsilon$  and whose ratio of lengths of tangent semi-axes and the normal semi-axes is  $q$ . We denote by  $R_\varepsilon(X)$  the Rips complex at scale  $\varepsilon$ . Then the following relation holds*

$$R_{\varepsilon/q}(X) \subset E_\varepsilon^q(X) \subset R_\varepsilon(X). \quad (2)$$

*Proof.* Let us denote by  $b := \frac{\varepsilon}{q}$ .

We first prove that  $R_b(X) \subset E_\varepsilon^q(X)$ . Let  $\sigma \in R_b(X)$ . This means that  $\forall x, y \in \sigma, d(x, y) \leq 2b$ . This, in particular, implies that  $B_b(x) \cap B_b(y) \neq \emptyset$ . Since  $B_b(x) \subset E_\varepsilon^q(x)$  and  $B_b(y) \subset E_\varepsilon^q(y)$  it follows that  $E_\varepsilon^q(x) \cap E_\varepsilon^q(y) \neq \emptyset$  for all  $x, y \in \sigma$ . Therefore  $\sigma \in E_\varepsilon^q(X)$ .

Now we prove that  $E_\varepsilon^q(X) \subset R_\varepsilon(X)$ . Let  $\sigma \in E_\varepsilon^q$ . This implies that  $E_\varepsilon^q(x) \cap E_\varepsilon^q(y) \neq \emptyset$  for all  $x, y \in \sigma$ . Let  $z \in E_\varepsilon^q(x) \cap E_\varepsilon^q(y)$ . Since  $E_\varepsilon^q(x) \subset B_\varepsilon(x)$  and  $E_\varepsilon^q(y) \subset B_\varepsilon(y)$ , it follows by triangle inequality that

$$d(x, y) \leq d(x, z) + d(z, y) \leq \varepsilon + \varepsilon = 2\varepsilon.$$

This implies that  $d(x, y) \leq 2\varepsilon$  for all  $x, y \in \sigma$  and therefore  $\sigma \in R_\varepsilon(X)$ .

Figure 4 shows the relation between ellipsoids used in the construction of the ellipsoid complex and the balls used for the Rips complex.

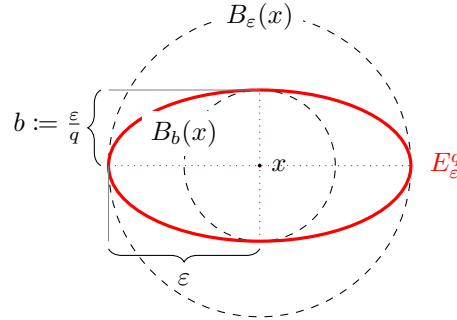


Figure 4: A graphical representation of the nesting property between balls (dashed circles) and ellipsoids (red) that implies the nesting relation between Rips and ellipsoid complexes.

□

## 3 Persistent Homology via Ellipsoids: the Algorithm

In this section we describe the algorithm to compute persistent homology via ellipsoid complexes. To store the ellipsoid complex and calculate its persistent homology, we use a *simplex tree* data structure [BM14] based on the GUDHI [Mar23]. More specifically, we do the following:

---

**Algorithm 2** Calculating barcodes from ellipsoid complexes

---

**Require:** Point cloud, user-chosen axes ratios of ellipsoids

```
1: Use Algorithm 1 to obtain a list of ellipsoids.
2:  $S \leftarrow \emptyset$  ▷ Initialise empty simplex tree
3: for each point  $p$  in the point cloud do
4:   for each point  $q$  in the point cloud do
5:      $r \leftarrow \text{find\_intersection\_radius}(E_\bullet^q(p), E_\bullet^p(q))$  ▷ Find radius at which ellipsoids intersect
6:      $S \leftarrow S \cup (\{p, q\}, r)$ 
7:   end for
8: end for
9:  $S.\text{expansion}()$  ▷ Expand flag complex
10:  $S.\text{persistence}()$  ▷ Calculate barcode
```

---

The complexity of the algorithm depends on the complexity of the algorithm used to first create the ellipsoids, which we earlier determined to be  $\mathcal{O}(nk \log n + n \min(d^3, k^3))$ . We recall that  $n$  refers to the number of sample points,  $d$  to their dimension, and  $k$  to the number of neighbours used for the tangent-space approximation. Algorithm 2 is thus *prima facie* dominated by the nested loops, which check for all intersections between ellipsoids, for which we use a pre-existing algorithm [htt; GH12] that we outline below for the reader's convenience. Assuming that this step has *constant* complexity, checking all pairwise intersections has a complexity of  $\mathcal{O}(n^2)$ . The expansion of the flag complex (executed in the penultimate line) has *output-sensitive complexity* and is trivially upper-bounded by  $\mathcal{O}\left(\binom{n}{2}\right)$ ; see [BM14] for a more detailed analysis. Finally, the barcode calculation takes at most  $\mathcal{O}(m^\omega)$  time, where  $m$  denotes the size of the resulting flag complex, and  $\omega = 2.376$  denotes the best bound for matrix multiplication [MMS11]. Since our algorithm shares the last two steps with standard persistent-homology algorithms, improvements of the (practical) runtime require replacing the intersection checks. We leave this for future work, noting that classical results on improving the performance of rigid-body simulations [BW92] could potentially be gainfully combined with improved flag complex expansion algorithms [Zom10].

### 3.1 Intersection of Ellipsoids

We first recall the definition of an ellipsoid given by equation (1). In this definition it is assumed that the axes of the ellipsoid are aligned with the coordinate axes. We can rewrite equation (1) as:

$$E_\varepsilon^q(x) = \{(x_1, \dots, x_n) \in \mathbb{R}^n \mid (x_1, \dots, x_n)^T \Lambda (x_1, \dots, x_n) = 1\},$$

for  $\Lambda$  a diagonal matrix whose diagonal entries  $\lambda_1, \dots, \lambda_n$  are given by  $\lambda_1 = \dots = \lambda_m = \frac{1}{\varepsilon^2}$  and  $\lambda_{m+1} = \dots = \lambda_n = \frac{1}{b^2}$ . To rotate such an ellipsoid so that its axes lie along the orthonormal basis  $\{v_1, \dots, v_n\}$ , we can apply a rotation matrix  $P$  sending the coordinate axes  $e_1, \dots, e_n$  to  $v_1, \dots, v_n$ . In other words, the matrix  $P$  is given by

$$P = \begin{pmatrix} | & & | \\ v_1 & \dots & v_n \\ | & & | \end{pmatrix},$$

so that  $Pe_i = v_i$ . The equation describing an ellipsoid centered at a point  $p \in \mathbb{R}^n$  with the axes given by the vectors  $v_i \in \mathbb{R}^n$ ,  $i \in \{1, \dots, n\}$  can thus be written as follows:

$$\{x \in \mathbb{R}^n \mid (P^{-1}(x-p))^T \Lambda P^{-1}(x-p) \leq 1\} \stackrel{(\spadesuit)}{=} \{x \in \mathbb{R}^n \mid (x-p)^T P \Lambda P^T (x-p) \leq 1\}. \quad (3)$$

In equality  $(\spadesuit)$ , we used the fact that rotation matrices are orthogonal, i.e.  $P^{-1} = P^T$ .

In determining whether two ellipsoids intersect, it is important to keep track of their orientations. For this reason, in the next proposition, we denote by  $E(P \Lambda P^T, p)$  the ellipsoid  $E_\varepsilon^q(p)$  with axes lying along the unit vectors  $Pe_1, \dots, Pe_n$ , where  $P$  is a rotation matrix and  $e_1, \dots, e_n$  are the coordinate axes. As above,

the matrix  $\Lambda$  is the diagonal matrix with the diagonal entries  $\lambda_1, \dots, \lambda_n$  equal to the squared reciprocals of the axes lengths, i.e.  $\lambda_1 = \dots = \lambda_m = \frac{1}{\varepsilon^2}$  and  $\lambda_{m+1} = \dots = \lambda_n = \frac{q^2}{\varepsilon^2}$ . We use the following result to determine whether two ellipsoids intersect:

**Proposition 3.1** ([GH12, Proposition 2]). *Let  $E(A, c)$  and  $E(B, d)$  be two ellipsoids (here we use the notation described in the previous paragraph). Denote  $v = d - c$  and define*

$$K: [0, 1] \rightarrow \mathbb{R}, \quad \lambda \mapsto 1 - v^T \left( \frac{1}{1-\lambda} B^{-1} + \frac{1}{\lambda} A^{-1} \right)^{-1} v. \quad (4)$$

The ellipsoids  $E(A, c)$  and  $E(B, d)$  intersect if and only if for all  $\lambda \in (0, 1)$  we have  $K(\lambda) > 0$ .

Thus, given two ellipsoids  $E(A, c)$  and  $E(B, d)$ , we find the minimum of the function  $K$  as defined in equation (4). If the minimum is smaller than 0, the two ellipsoids intersect. Since the objective function is convex, the problem is feasible and convergence is guaranteed, enabling the use of efficient optimisation procedures [Vir+20].

## 4 Experiments

We present an experimental suite whose primary goal is to highlight the differences between Rips complexes and ellipsoids complexes. Our experiments aim to answer when ellipsoids barcodes are more *expressive* than Rips barcodes, i.e., in which situations an ellipsoid barcode uncovers *more* information about a dataset than a Rips barcode and to demonstrate that using ellipsoids one can get valuable information from smaller samples. To this end we provide a visual analysis of both types of barcodes on synthetic and real-world datasets (conformation space of cyclo-octane), followed by several *classification experiments*. For the latter, we draw on previous work [TMO22] to obtain a setting in which the performance of Rips barcodes (and derived topological descriptors) is already well-studied.

### 4.1 Dog Bone Example

Examples where ellipsoids are advantageous compared to Rips complexes include spaces with bottlenecks (as already remarked in [Bre+18] for ellipsoid-driven complexes). For example, consider a curve in the shape of a dog bone. Figure 5 represents ellipsoids for  $q = 3$  at different scales:  $\varepsilon = 0.1, \varepsilon = 0.2$  and  $\varepsilon = 0.6$ .

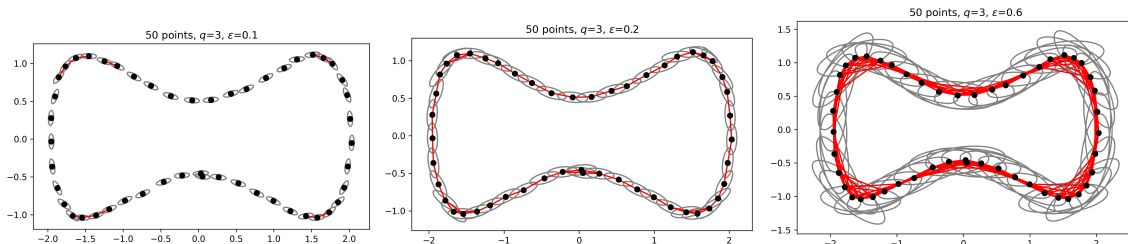


Figure 5: Ellipsoids complexes for  $q = 3$  at scales  $\varepsilon = 0.1, \varepsilon = 0.2$  and  $\varepsilon = 0.6$  for a point cloud sampled from a curve resembling a dog bone.

In cases like this dataset the balls around points on the bottleneck may intersect for  $\varepsilon$  smaller than that which is necessary for the full cycle to appear. This is demonstrated in Figure 6. The ellipsoid barcode has one long bar in 1-dimensional homology, whereas the Rips barcode shows two prominent features.

### 4.2 Point Cloud Classification

To test how the classification based on the ellipsoid simplex compares to other methods, we run experiments analogous to ones described in [TMO22]. We generate point clouds of 20 different shapes in  $\mathbb{R}^2$  and  $\mathbb{R}^3$  with



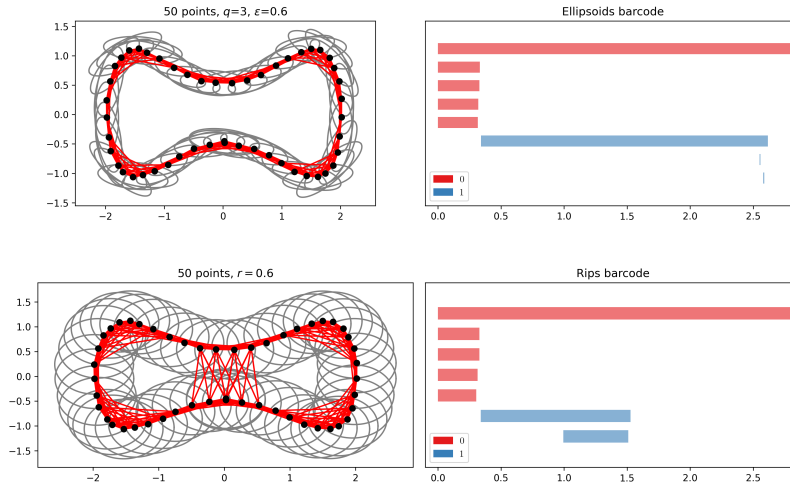


Figure 6: Top left: Ellipsoids for  $q = 3$  at scale  $\varepsilon = 0.6$ . Bottom left: Rips complex for  $q = 3$  at  $\varepsilon = 0.6$ . Top right: Ellipsoid barcode. Bottom Right: Rips barcode.

four different shapes having the same number of holes (0, 1, 2, 4 or 9) (see Table 1 on the left for some examples).

For each shape, we generate 5 different point clouds, each consisting of 301 points. Note that in [TMO22], 1000 points were used. Due to the property of ellipsoids to approximate the underlying manifold structure of point clouds, we expect the classification accuracy to remain high even with the lower resolutions datasets. We have therefore decided to reduce sampling to 301 points per point cloud.

The experiments consist of classifying point clouds in  $\mathbb{R}^2$  and  $\mathbb{R}^3$  via different methods:

1. Using barcodes coming from ellipsoid complexes. We refer to this pipeline in the text as PHE.
2. Using barcodes coming from Rips complexes (PHR).
3. Using barcodes coming from alpha complexes generated using Distance-to-Measure as the filtration function (PH). As noted in [TMO22, Section 2.2], the filtration function used in Rips complex is sensitive to outliers, and to mitigate this limitation, the so-called Distance-to-Measure function is used instead. This function measures the average distance from a number of neighbours on the point cloud.
4. Using only the 10 longest lifespans in the barcodes coming from alpha complexes generated using Distance-to-Measure as the filtration function (PH simple).
5. Support vector machine trained on the distance matrices of point clouds (ML).
6. Fully connected neural network with a single hidden layer (NN shallow).
7. Fully connected neural network with multiple layers (NN deep).
8. PointNet [Cha+17].

To perform the PHE classification, i.e. the classification based on the ellipsoids data, we calculate the barcodes corresponding to the ellipsoids complex and then use the remainder of the PH pipeline developed in [TMO22]. In particular, we feed a support vector machine with a signature calculated from the ellipsoid barcode. We choose this signature amongst the following:

- (a) signature containing 10 longest lifespans;

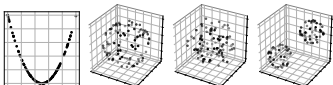
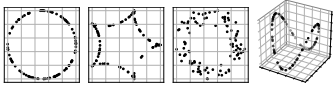
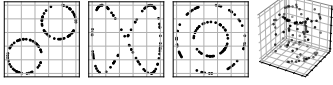
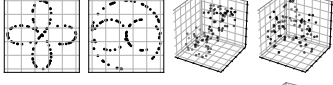

No. holes	Example point clouds	Transformation name	Explanation
		original	The original dataset.
		translation	Translation by random numbers chosen from $[-1, 1]$ for each direction.
0		rotation	Clockwise rotation by an angle chosen uniformly from $[-20, 20]$ degrees clockwise.
1		stretch	Scale by a factor chosen uniformly from $[0.8, 1.2]$ in the $x$ -direction leaving the other coordinates unchanged.
2		shear	Shear by a factor chosen uniformly from $[-0.2, 0.2]$ . A shearing factor of 1 means that a horizontal line turns into a line at 45 degrees.
4		Gaussian noise	Random noise drawn from normal distribution $\mathcal{N}(0, \sigma)$ with the standard deviation $\sigma$ uniformly chosen from $[0, 0.1]$ is added to the point cloud.
9		outliers	A percentage, chosen uniformly from $[0, 0.1]$ , of point cloud points are replaced with points sampled from a uniform distribution within the range of the point cloud.

Table 1: Left: Example point clouds of the ‘holes’ data set [TMO22]. Our experiments assess to what extent predictions of the number of holes also work with fewer points. Right: Explanations of the data transformations used on the datasets

(b) persistence images (generated by choosing various different parameters) [Ada+17];

(c) persistence landscapes (generated by choosing various different parameters) [Bub15].

Whichever option between (a), (b) or (c) (with whichever combination of parameters) leads to the highest score, i.e., accuracy, is then used as a signature in the actual classification. This means that, depending on the datasets, different signatures might be used on the ellipsoids barcodes.

In the PHR pipeline, i.e. the classification based on the Rips complexes we perform the same steps, except that we use the barcodes coming from the Rips complex.

The experiments test the classification of the original datasets, as well as of the datasets after various transformations have been applied to them: translation, rotation, stretching, shear mapping, adding Gaussian noise, and replacing a certain number of points with outliers. In Table 1 we reproduce the table from [TMO22] explaining these transformations in more detail.

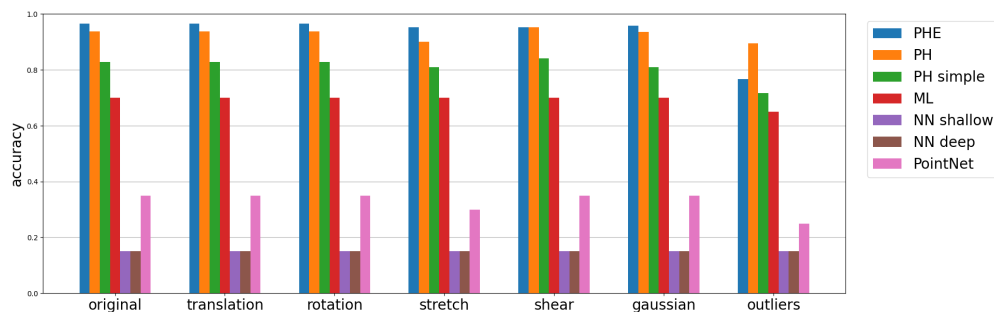


Figure 7: Classification accuracies.

The results shown in Figure 7 represent average accuracies over 23 runs of the classification pipeline on the same dataset in its original state, as well as after the transformations have been applied to it. The ratio between the training data and the test data remains fixed, but the test and the training data change.

The classification based on ellipsoids data performs best in all cases, except when outliers are introduced to the point cloud.

We also perform classification based on Rips barcodes and the obtained accuracies are shown in Figure 8. As expected, Rips barcodes lead to worse results.

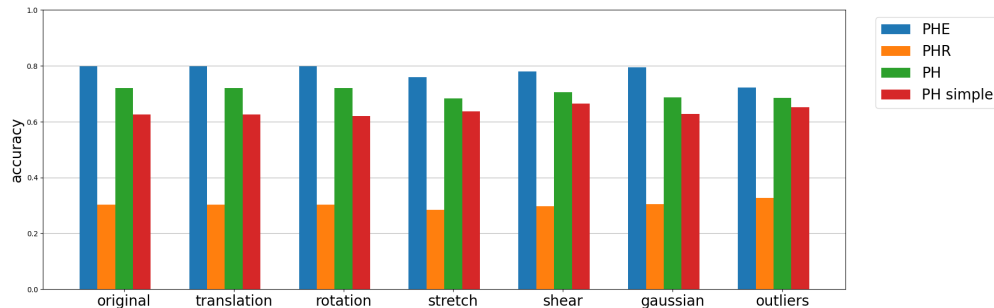


Figure 8: Classification accuracies.

The code used in this subsection is available at <https://github.com/a-zeg/ellipsoids>. Computations of the ellipsoids barcodes were performed on the ETH Zürich Euler cluster, whereas the subsequent classification was performed on 1.1 GHz Quad-Core Intel Core i5.

### 4.3 Pentagons

As the next example, consider a dataset of 14074 points from the configuration space of the space of equilateral planar pentagons, viewed as living in  $\mathbb{R}^6$ . More precisely, the dataset consists of a sample of 14074 points from

$$M = \{(x_1, x_2, x_3) \in \mathbb{R}^6 \mid \|x_i - x_{i+1}\|, i = 1, 2, 3, 4, 5\},$$

where  $x_4$  and  $x_5$  are fixed vectors in  $\mathbb{R}^2$  and where we regard  $x_6$  as  $x_1$ . The dataset was created by Clayton Shonkwiler and provided to us by Henry Adams.

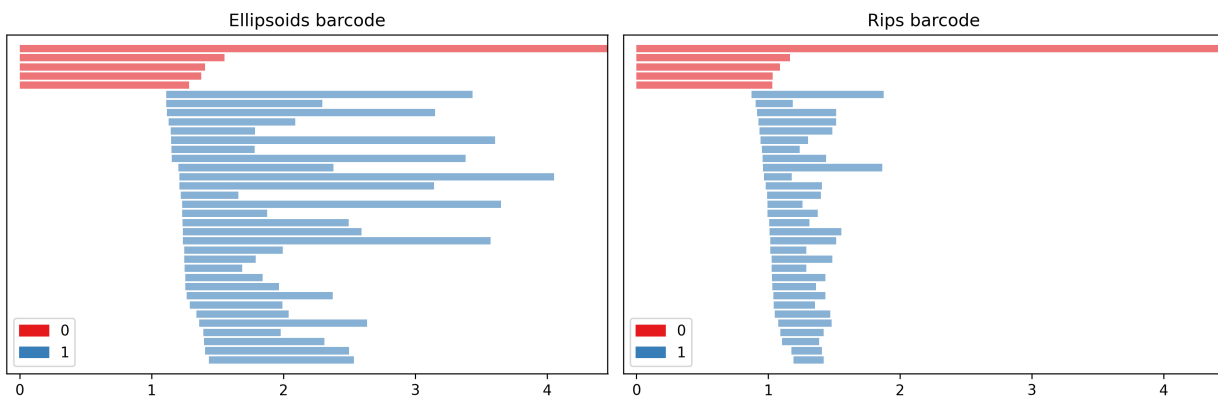


Figure 9: In some cases, even when the pentagons dataset is downsampled to only 100 points, we can see that the ellipsoids barcode captures the correct Betti numbers.

It was established in [Hav91] that  $M$  is a compact, connected and orientable, two-dimensional manifold of genus 4. We tested this hypothesis with persistent homology via ellipsoids and Rips complexes. Ellipsoids can detect the ‘correct homology’ with a subsample consisting of as few as 100 points (see Figure 9).

## 4.4 Cyclo-octane

The last example for which we compare the ellipsoid and Rips barcodes is for the conformation space of the cyclo-octane dataset. The cyclo-octane dataset was introduced in [Mar+10] and consists of 6040 points in 24 dimensions. It is publicly available as part of the javaPlex [TVA14] software package.

A single molecule of the cyclo-octane consists of eight carbon atoms arranged in a ring, with each carbon atom being bound to two other carbon atoms and two hydrogen atoms. The location of the hydrogen atoms is determined by that of the carbon atoms due to energy minimization. Hence, the conformation space of cyclo-octane consists of all possible spatial arrangements, up to rotation and translation, of the ring of carbon atoms (see the left image in Figure 10). Each conformation may therefore be represented by a point in  $\mathbb{R}^{24}$ , where we have three spatial coordinates for each of the eight carbon atoms. Brown et al. [Bro+08] and Martin et al. [Mar+10] show that the conformation space of cyclo-octane is the union of a sphere with a Klein bottle, glued together along two circles of singularities (see the right image in Figure 10).

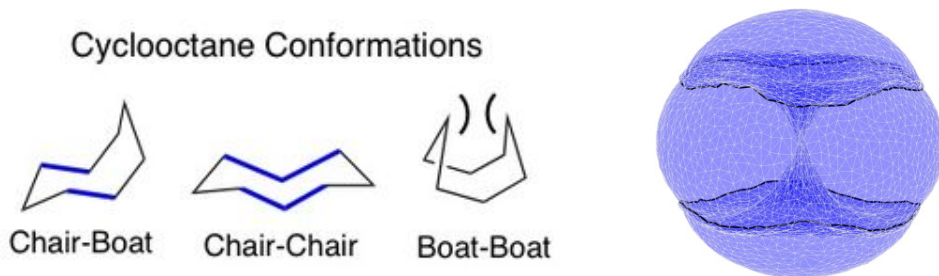


Figure 10: Left: Examples of Cyclooctane Conformations. Right: The conformation space of cyclo-octane is the union of a sphere with a Klein bottle, glued together along two circles of singularities. The picture is taken from [Mar+10].

The cyclo-octane dataset has been used many times as an example to show that we can recover the homology groups of the conformation space using persistent homology [Zom12; TVA14]. We confirmed this result using ellipsoid complexes. The results for a 500-point subsample are displayed in Figure 11. The barcodes from the usual Vietoris–Rips complex do not capture the correct homology groups, whereas the ellipsoid barcodes do. In particular, where 2-dimensional Rips barcode only shows noise, the ellipsoid barcode has two prominent bars.

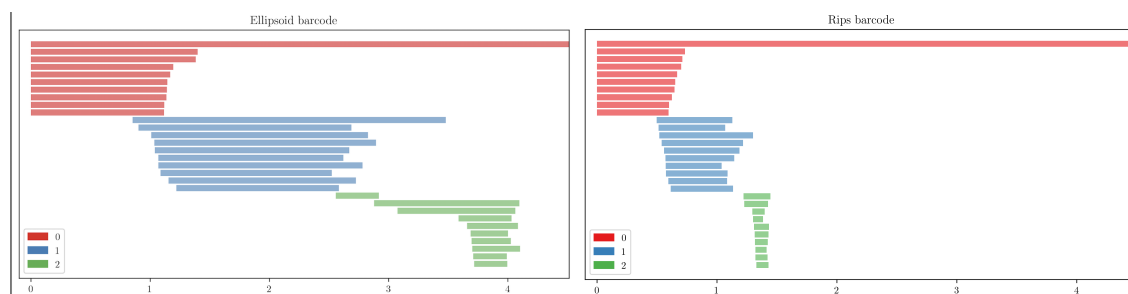


Figure 11: Barcodes for a subsample of 500 points from the cyclo-octane dataset. The right plot shows the barcodes for the usual Vietoris–Rips complex. The left picture shows barcodes for the ellipsoid complex.

## 5 Conclusion and Future Directions

Previous experiments [Bre+18] and theoretical results [KL24] support the statement that using shapes elongated along tangent directions one can reduce the size of the sample from a manifold while still capturing its shape.

In this paper we present code (available at <https://github.com/a-zeg/ellipsoids>) for computing persistent homology with such elongated shapes, the so called ellipsoid complexes, where simplices are included based on intersections of ellipsoids, not balls. These ellipsoids can be constructed for a general point cloud (in contrast with [Bre+18], where samples were drawn from varieties). We also present the results of extensive experiments where we compare ellipsoid barcodes with Rips barcodes. In particular, we show that:

- Working with ellipsoids is particularly suitable when the underlying spaces has bottlenecks (as demonstrated in Subsection 4.1) or is a manifold.
- Since ellipsoids better approximate the underlying manifold structure of data than balls, their barcodes lead to better classification results in sparsely sampled point clouds and, in general, allow the user to work with smaller samples.
- Using the datasets from [TMO22] we show that ellipsoid barcodes outperform alpha barcodes for classification purposes (see Subsection 4.2) in all categories except one.

These points demonstrate the strengths of working with ellipsoid complexes. The slower computational time is partly offset by the much smaller sample size needed to still capture homology groups compared to the Rips complex.

There are several questions left to be addressed: for example, how to optimize the code for more efficient computation of ellipsoid complexes and equally important, to prove a stability result for these types of complexes. Another future direction is to use ellipsoids in construction of alpha complexes to reduce the size of the simplicial complexes in the filtration.

## 6 Acknowledgements

We thank Henry Adams for providing us with the pentagons dataset and Clayton Shonkwiler for creating it. A.Z. would like to thank Marco Gähler and Jan Schüssler for their help with the programming part of this project.

## References

- [Ada+17] H. Adams et al. “Persistence images: A stable vector representation of persistent homology”. In: *Journal of Machine Learning Research* 18.8 (2017), pp. 1–35.
- [Bau+22] U. Bauer et al. “A unified view on the functorial nerve theorem and its variations”. In: *Expositiones Mathematicae* (2022).
- [BM14] J.-D. Boissonnat and C. Maria. “The Simplex Tree: An Efficient Data Structure for General Simplicial Complexes”. In: *Algorithmica* 70.3 (2014), pp. 406–427. DOI: 10.1007/s00453-014-9887-3.
- [Bre+18] P. Breiding et al. “Learning algebraic varieties from samples”. In: *Revista Matemática Complutense* 31.3 (Sept. 2018), pp. 545–593. DOI: 10.1007/s13163-018-0273-6.
- [Bro+08] W. M. Brown et al. “Algorithmic dimensionality reduction for molecular structure analysis”. In: *The Journal of Chemical Physics* 129.6 (Aug. 2008), p. 064118. DOI: 10.1063/1.2968610.
- [Bub15] P. Bubenik. “Statistical topological data analysis using persistence landscapes.” In: *Journal of Machine Learning Research* 16.1 (2015), pp. 77–102.

- [BW92] D. Baraff and A. Witkin. “Dynamic simulation of non-penetrating flexible bodies”. In: *Proceedings of the 19th Annual Conference on Computer Graphics and Interactive Techniques*. New York, NY, USA: Association for Computing Machinery, 1992, pp. 303–308. DOI: 10.1145/133994.134084.
- [Car09] G. Carlsson. “Topology and Data”. In: *Bulletin of the American Mathematical Society* 46 (2009), pp. 255–308.
- [Car13] G. Carlsson. “Topological pattern recognition for point cloud data”. In: *Acta Numerica* 23 (2013), pp. 289–368.
- [Cha+16] F. Chazal et al. *The Structure and Stability of Persistence Modules*. Heidelberg, Germany: Springer, 2016.
- [Cha+17] R. Q. Charles et al. “PointNet: Deep Learning on Point Sets for 3D Classification and Segmentation”. In: *IEEE Conference on Computer Vision and Pattern Recognition (CVPR)*. 2017, pp. 77–85. DOI: 10.1109/CVPR.2017.16.
- [CSO14] F. Chazal, V. de Silva, and S. Oudot. “Persistence stability for geometric complexes”. In: *Geometriae Dedicata* 173 (2014), pp. 193–214. DOI: 10.1007/s10711-013-9937-z.
- [DI12] S. Dantchev and I. Ivrišimtzis. “Efficient construction of the Čech complex”. In: *Computers & Graphics* 36.6 (2012), pp. 708–713. DOI: 10.1016/j.cag.2012.02.016.
- [ELZ02] H. Edelsbrunner, D. Letscher, and A. J. Zomorodian. “Topological persistence and simplification”. In: *Discrete and Computational Geometry* 28 (2002), pp. 511–533.
- [FH16] M. S. Fefferman C. and N. H. “Testing the manifold hypothesis”. In: *Journal of the American Mathematical Society* 29 (2016), pp. 983–1049. DOI: 10.1090/jams/852.
- [FS10] M. Ferri and I. Stanganelli. “Size Functions for the Morphological Analysis of Melanocytic Lesions”. In: *International Journal of Biomedical Imaging* 2010 (2010).
- [GH12] I. Gilitschenski and U. D. Hanebeck. “A robust computational test for overlap of two arbitrary-dimensional ellipsoids in fault-detection of Kalman filters”. In: *15th International Conference on Information Fusion*. 2012, pp. 396–401.
- [Hat02] A. Hatcher. *Algebraic topology*. Cambridge, UK: Cambridge University Press, 2002.
- [Hav91] T. F. Havel. “Some examples of the use of distances as coordinates for Euclidean geometry”. In: *Journal of Symbolic Computation* 11.5 (1991), pp. 579–593. DOI: 10.1016/S0747-7171(08)80120-4.
- [htt] N. A. (<https://math.stackexchange.com/users/3060/nick-alger>). *Detect if two ellipses intersect*. URL: <https://math.stackexchange.com/q/3678498>.
- [JC16] I. T. Jolliffe and J. Cadima. “Principal component analysis: a review and recent developments”. In: *Philosophical Transactions of the Royal Society A: Mathematical, Physical and Engineering Sciences* 374 (2016).
- [JL09] I. M. Johnstone and A. Y. Lu. “On Consistency and Sparsity for Principal Components Analysis in High Dimensions”. In: *Journal of the American Statistical Association* 104.486 (2009), pp. 682–693. DOI: 10.1198/jasa.2009.0121.
- [KL24] S. Kališnik and D. Lešnik. “Finding the homology of manifolds using ellipsoids”. In: *Journal of Applied and Computational Topology* 8.1 (Mar. 2024), pp. 193–238. DOI: 10.1007/s41468-023-00145-6.
- [Mar+10] S. Martin et al. “Topology of cyclo-octane energy landscape”. In: *The Journal of Chemical Physics* 132.23 (June 2010), p. 234115. DOI: 10.1063/1.3445267.
- [Mar23] C. Maria. “Filtered Complexes”. In: *GUDHI User and Reference Manual*. 3.8.0. GUDHI Editorial Board, 2023.

- [MMS11] N. Milosavljević, D. Morozov, and P. Skraba. “Zigzag persistent homology in matrix multiplication time”. In: *Proceedings of the Twenty-Seventh Annual Symposium on Computational Geometry*. SoCG. New York, NY, USA: Association for Computing Machinery, 2011, pp. 216–225. DOI: 10.1145/1998196.1998229.
- [Rob00] V. Robins. “Computational topology at multiple resolutions.” PhD thesis. University of Colorado, 2000.
- [TMO22] R. Turkeš, G. F. Montúfar, and N. Otter. “On the Effectiveness of Persistent Homology”. In: *Advances in Neural Information Processing Systems*. Ed. by S. Koyejo et al. Vol. 35. Curran Associates, Inc., 2022, pp. 35432–35448.
- [TVA14] A. Tausz, M. Vejdemo-Johansson, and H. Adams. “JavaPlex: A research software package for persistent (co)homology”. In: *Proceedings of ICMS 2014*. Ed. by H. Hong and C. Yap. Lecture Notes in Computer Science 8592. Software available at <http://appliedtopology.github.io/javaplex/>. 2014, pp. 129–136.
- [Vir+20] P. Virtanen et al. “SciPy 1.0: Fundamental Algorithms for Scientific Computing in Python”. In: *Nature Methods* 17 (2020), pp. 261–272. DOI: 10.1038/s41592-019-0686-2.
- [Zom10] A. Zomorodian. “Fast construction of the Vietoris-Rips complex”. In: *Computers & Graphics* 34.3 (2010), pp. 263–271. DOI: 10.1016/j.cag.2010.03.007.
- [Zom12] A. Zomorodian. *Advances in Applied and Computational Topology*. USA: American Mathematical Society, 2012.